Supplementary Information

Water-plasma-assisted synthesis of black titania spheres with efficient visible-light photocatalytic activity

Gasidit Panomsuwan,*[a] Anyarat Watthanaphanit,[bc] Takahiro Ishizaki[ae] and Nagahiro Saito[bcde]

[a] Department of Materials Science and Engineering, Faculty of Engineering, Shibaura Institute of Technology, Tokyo 135-8548, Japan

[b] Social Innovation Design Center (SIDC), Institute of Innovation for Future Society, Nagoya University, Nagoya 464-8603, Japan

[c] Department of Materials, Physics and Energy Engineering, Graduate School of Engineering, Nagoya University, Nagoya 464-8603, Japan

[d] Green Mobility Collaborative Research Center, Nagoya University, Nagoya 464-8603, Japan

[e] Core Research for Evolutional Science and Technology (CREST), Japan Science and Technology Agency (JST), Saitama 332-0012, Japan

*Corresponding author

Gasidit Panomsuwan

Department of Materials Science and Engineering, Faculty of Engineering,

Shibaura Institute of Technology, 3-7-5 Toyosu, Koto-ku, Tokyo 135-8548, Japan

Tel: +81-3-5859-8115

Fax: +81-3-5859-8101

E-mail: i036050@sic.shibaura-it.ac.jp, g.panomsuwan@gmail.com

Experimental section

Chemicals

Commercial TiO_2 (Aeroxide P25) was supplied by Nippon Aerosil Co., Ltd. Methylene blue ($C_{16}H_{18}N_3SCl$, purity ≥ 97%) and potassium chloride (KCl, purity ≥ 99%) were obtained from Sigma-Aldrich. Barium sulfate ($BaSO_4$), phenol (C_6H_6O, purity ≥ 99%), and ethanol (C_2H_6O, purity ≥ 99.5%) were obtained from Wako Pure Chemical Industries, Ltd. All of the chemicals were of analytical grade and used without further purification. Milli-Q ultrapure water (18.2 MΩ·cm) was obtained from a RFD250NB Aquarius water purification system and used throughout the experiment in this study.

Water-plasma-assisted synthesis of black H-TiO_{2-x} spheres

The preparation of H-TiO_{2-x} was performed in a Pyrex glass reactor, as schematically presented in Fig. S1. The 1 mm diameter Ti wire (Sigma-Aldrich, purity 99.99%) was used as the symmetric electrodes and placed at the center of the reactor. The Ti-pair electrodes were shielded with an insulating ceramic tube and fixed to the reactor by silicone stopper. The reactor contained an aqueous electrolyte solution (100 ml, 0.3 mM KCl, σ = 150 S·cm) in order to attain stable and continuous plasma. A high voltage was applied to the symmetric Ti-pair electrodes using a bipolar power supply (Kurita Co. Ltd., Japan). The pulse duration and frequency were fixed at 2 μs and 20 kHz, respectively. The current–voltage waveform of the water plasma is shown in Fig. S2. Once the applied voltage reached to breakdown point, the plasma was generated at the gap between the Ti electrodes. The reactor was immersed in a cooling bath under vigorous stirring in order to keep the temperature below 60 °C during synthesis. The optical emission spectrum of the plasma was recorded with an Avantes AvaSpec-3648 optical spectrometer in the wavelength range of 200 to 800 nm. The aqueous solution became turbid with light gray color within 15 min and then turned to dark-gray color with the prolongation of discharge time. The sample was separated from the aqueous solution by centrifugation and washed several times with ultrapure water. Finally, the sample was dried at 100 °C for 24 h in an open air to completely remove the water.

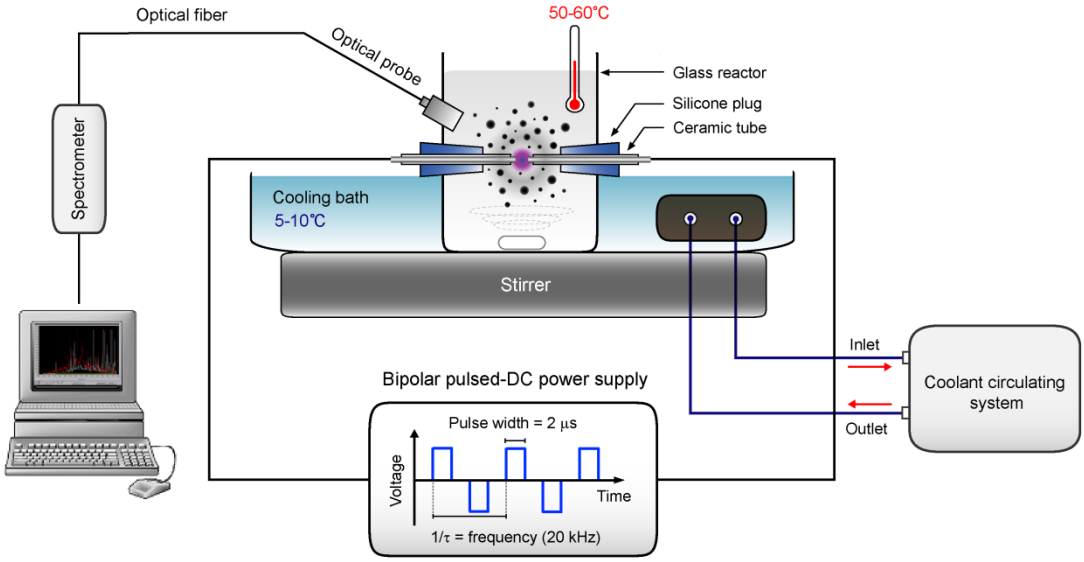

Fig. S1 Schematic illustration of experimental setup in this study.

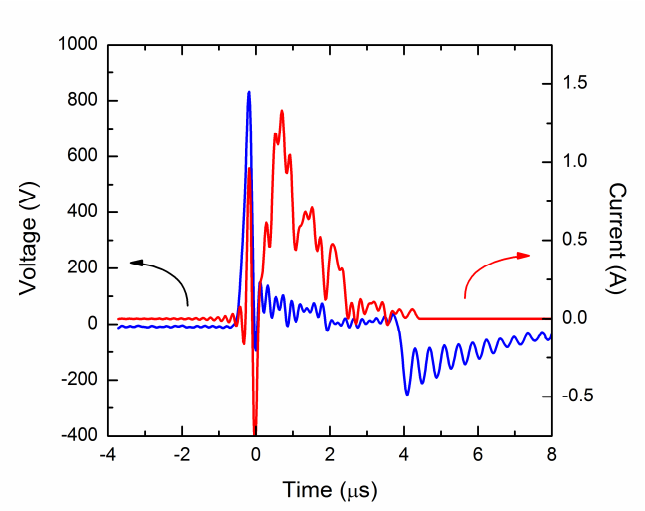

Fig. S2 A typical current and voltage waveform of the water plasma.

Characterizations

Diffuse reflectance spectroscopy (DRS): the finely ground samples were packed into the sample holder and then measured using a Shimadzu UV-3600 UV-vis-NIR spectrophotometer equipped with an integrated sphere accessory. Pure barium sulfate powder ($BaSO_4$) was used as a standard for background measurement. The reflectance spectra were converted to the equivalent absorption coefficient by Kubelka–Munk (K–M) function $F(R_\infty)$:

$$F(R) = \frac{(1-R)^2}{2R} = \frac{K}{S}$$

where R is the measured absolute reflectance from the infinitely thick samples ($R = R_{sample}/R_{standard}$), K is the absorption coefficient, and S is the scattering coefficient. $F(R)$ was used as the equivalent absorption coefficient on the assumption that the scattering coefficient was consistent throughout the compared samples. The band gap can be estimated from the intercept of extrapolated linear portion on the $h\nu$ axis of the plot of $[F(R)h\nu]^{1/2}$ *versus* $h\nu$.

Scanning electron microscopy (SEM): the morphology was observed with a JEOL JSM-6330F field-emission scanning electron microscope operating at an acceleration voltage of 10 kV.

Transmission electron microscopy (TEM): the morphology was investigated with a JEOL JEM-2500SE transmission electron microscope at an acceleration voltage of 200 kV. Dried powder samples was finely ground by agate mortar and then dispersed in ethanol under ultrasonic bath for 15 min. The suspension was dropped onto a 150 mesh copper TEM grid and let the solvent evaporation for 24 h prior to the measurement. More detailed information on structural properties was also obtained by high-resolution TEM investigation.

Brunauer-Emmett-Teller (BET) measurement: nitrogen adsorption-desorption isotherms were performed on a Belsorp-mini II at liquid nitrogen temperature (77 K). The relative pressure (P/P_0) was varied from 0 to 0.99. Prior to measurement, the samples were heated at 150 °C for 3 h under N_2 flow. The specific surface area was determined using the BET method at the relative pressure between 0.0 and 0.5. The pore volume and pore size distribution were determined using Barrett-Joyner-Halenda (BJH) method.

X-ray diffraction (XRD): the phase structure was identified using a Rigaku SmartLab X-ray diffractometer with monochromatic Cu Kα radiation (λ = 1.54 Å) operating at 45 kV and 200 mA (9 kW).

Raman spectroscopy: Raman spectra were recorded on a JASCO NRS-1000 Raman spectrometer using an excitation wavelength of 532.1 nm. The samples were pressed into pellet form for the measurement.

X-ray photoelectron spectroscopy (XPS): the chemical bonding state of the samples was acquired on a JEOL JPS-9010MC with monochromatic Mg Kα radiation (1253.6 eV) as an excitation source. The emission current and anode voltage were operated at 25 mA and 10 kV, respectively. The binding energy (BE) was calibrated using the C 1s peak (284.5 eV). The relevant fitting curves were analyzed using a Gaussian line shape and Shirley background subtraction.

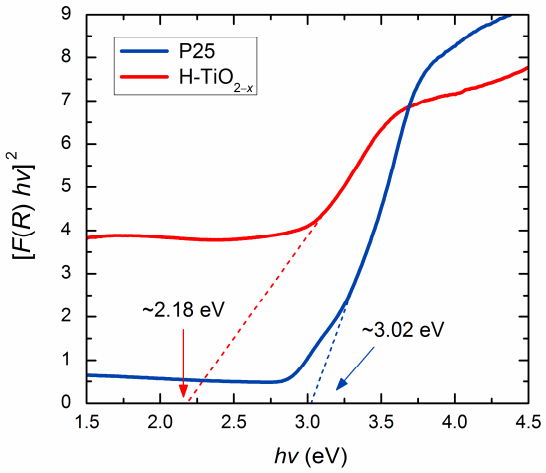

Fig. S3 Tauc plots of $[F(R)hv]^2$ *versus* hv for P25 and H-TiO_{2-x}. The band gap can be estimated by the extrapolation of the linear portion to the hv axis (indicated as dashed line).

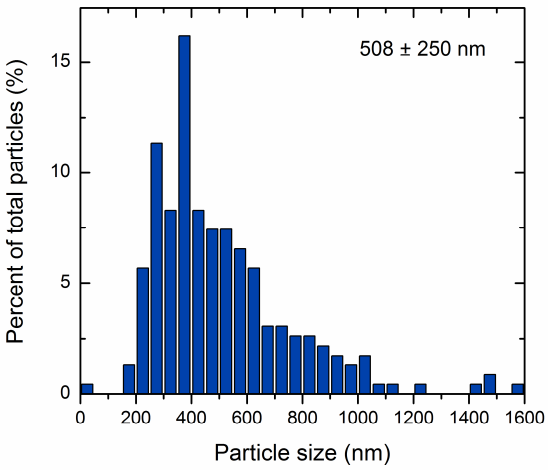

Fig. S4 Particle size distribution of H-TiO_{2-x} deduced from five hundred particles

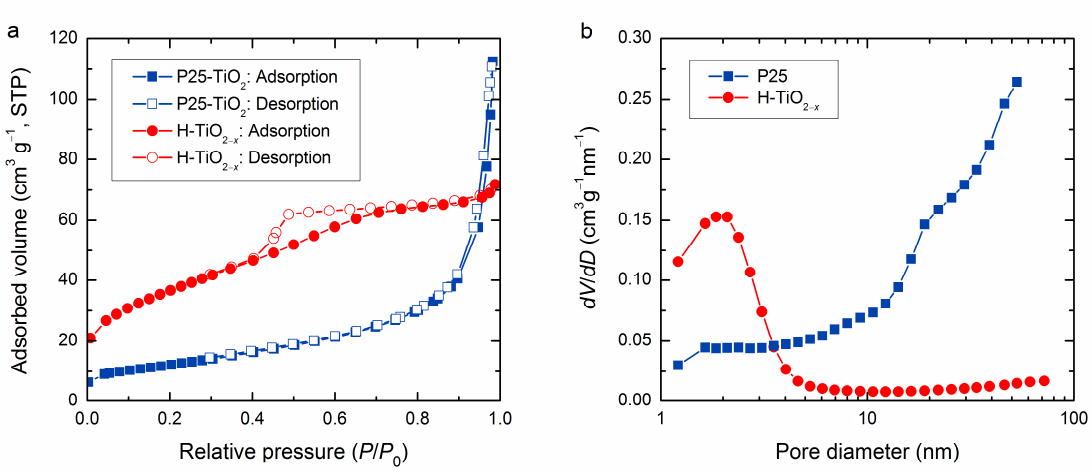

Fig. S5 (a) N_2 adsorption-desorption isotherms and (b) pore size distribution of P25 and H-TiO_{2-x} determined using the Barrett-Joyner-Halenda (BJH) method.

Table S1 Surface area, pore volume, and average pore diameter of P25 and H-TiO_{2-x}.

Sample	Surface area (m^2 g^{-1})	Pore volume (cm^3 g^{-1})	Pore diameter (nm)
P25	42.5	0.17	53.04
H-TiO_{2-x}	120.0	0.09	1.85

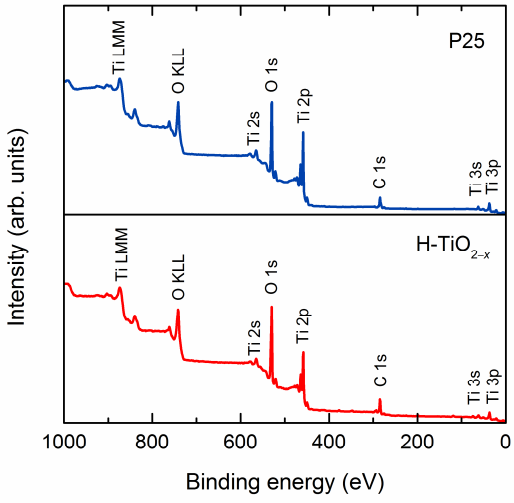

Fig. S6 XPS survey spectra of P25 and H-TiO_{2-x}.

Table S2 Detailed deconvolution of high-resolution XPS Ti 2p and O1s spectra for P25 and H-TiO_{2-x}.

Elemental bonding state		P25	H-TiO_{2-x}
O 1s	Ti^{2+}–O	-	528.3 eV (21.2%)
	Ti^{4+}–O	529.8 eV (89.7%)	529.8 eV (61.4%)
	Ti^{3+}–O	531.1 eV (8.1%)	531.1 eV (14.8%)
	Ti–OH	532.2 eV (2.2%)	532.3 eV (2.6%)
Ti 2p	Ti $2p_{3/2}$ (Ti^{4+})	458.6 eV	458.5 eV (47.0%)
	Ti $2p_{3/2}$ (Ti^{3+})		457.2 eV (18.0%)
	Ti $2p_{3/2}$ (Ti^{2+})		456.2 eV (2.9%)
	Ti $2p_{1/2}$ (Ti^{4+})	464.2 eV	464.2 eV (22.9%)
	Ti $2p_{1/2}$ (Ti^{3+})	-	462.9 eV (7.2%)
	Ti $2p_{1/2}$ (Ti^{2+})	-	461.9 eV (2.0%)

Photocatalytic activity measurements

Degradation of methylene blue dye: Photocatalytic activity of P25 and H-TiO_{2-x} was evaluated by the degradation of methylene blue (MB) as a representative organic pollutant. The 5 ppm of MB solution (5 mg L^{-1}, 1.35×10^{-5} M) was prepared and magnetically stirred under the dark conditions for 24 h in order to obtain absorption-desorption equilibrium. The 10 mg of sample was suspended in a Pyrex beaker containing 100 ml of 5 ppm MB solution. The suspension was magnetically stirred in the absence of light (dark condition) for 60 min to ensure an adsorption-desorption equilibrium between the photocatalyst and MB prior to light irradiation. After that, the suspension was irradiated by a 150 W xenon lamp (Hamamatsu Photonics K.K.) equipped with an aluminum mirror and a 420 nm cut-off filter (Hoya L-42). Two millimeter of suspension was collected every 20 min interval time and then centrifuged to separate the photocatalyst from the MB solution. The decolorization of MB solution was monitored by the variation of maximum absorption band at wavelength of 664 nm using a Shimadzu UV-3600 UV-Vis-NIR spectrophotometer.

Recycling test: After photocatalytic test, the suspensions were allowed to settle for 1 h for gravity sedimentation of the suspended H-TiO_{2-x}. The clear transparent MB solution was obtained and H-TiO_{2-x} was settled on the bottom of the reactor. Subsequently, H-TiO_{2-x} was collected and washed with ultrapure water for several times to remove residual ions and molecules. The cleaned H-TiO_{2-x} was then dried at 90 °C for 12 h prior to use for the recycle test. The recycle test was carried out for four times with the same procedure to confirm the stability of H-TiO_{2-x}. It is noted that H-TiO_{2-x} could

be easily separated from the solution compared to P25, which is of great advantage for the use of H-TiO_{2-x} in recycling process.

Degradation of phenol solution: Photocatalytic activity of H-TiO_{2-x} was also investigated by the degradation of a colorless phenol solution. In the experiment, 10 mg of H-TiO_{2-x} was added into a reactor containing 50 mL of phenol solution with an initial concentration of 5 mg L^{-1} (5.31×10^{-5} M). The suspension was magnetically stirred in the absence of light (dark condition) for 60 min to ensure an adsorption-desorption equilibrium prior to light irradiation. After that, the suspension was irradiated by a 150 W xenon lamp equipped with a 420 nm cut-off filter. The photocatalytic degradation was evaluated by the concentration changes of phenol solution at various irradiation times (determined from its characteristic absorption peak at 270 nm).

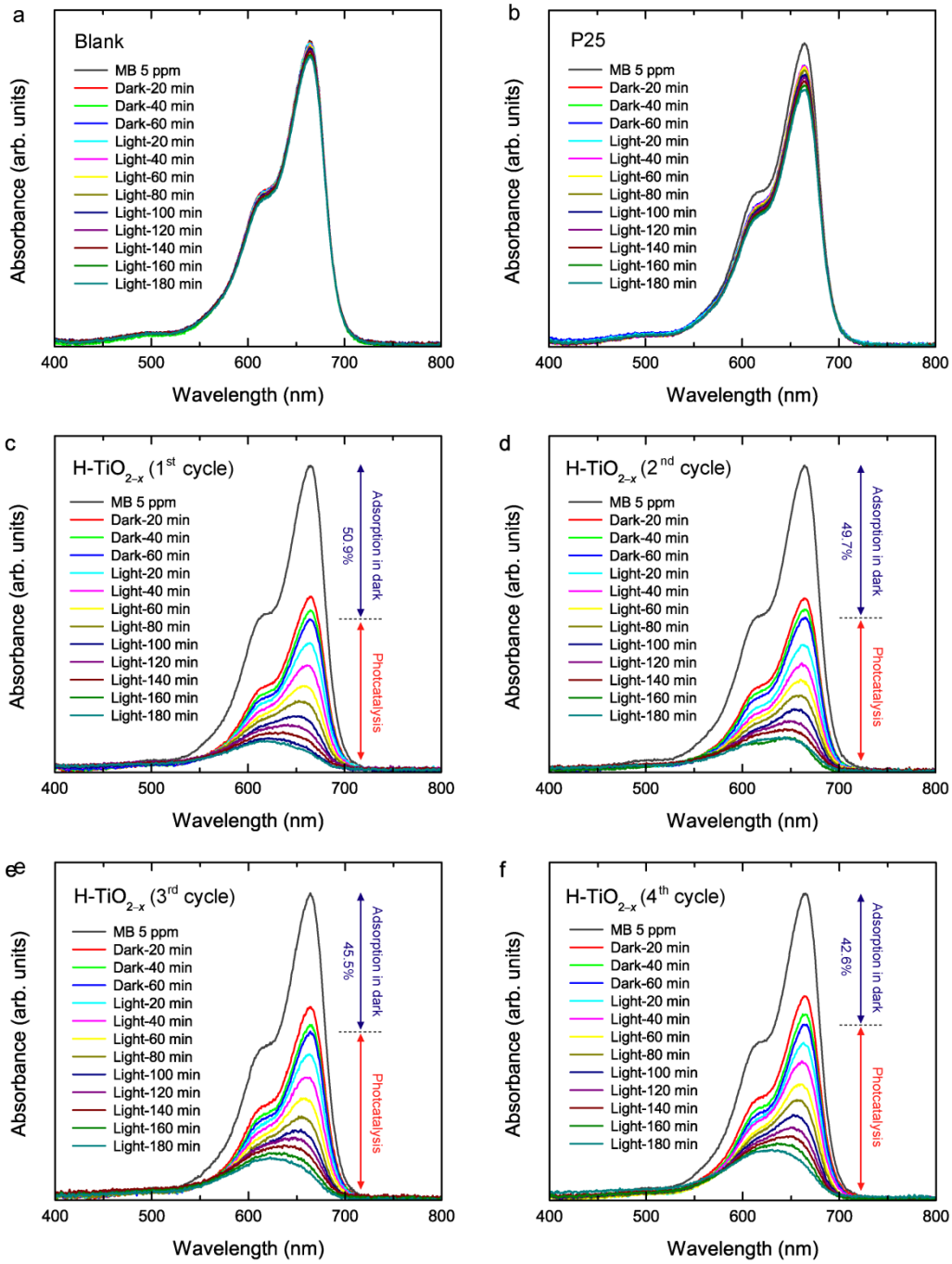

Fig. S7 UV-visible absorption spectra of MB solution at various irradiation times: (a) without photocatalyst, (b) P25, (c) H-TiO_{2-x} (1^{st} cycle), (d) H-TiO_{2-x} (2^{nd} cycle), (e) H-TiO_{2-x} (3^{rd} cycle), and (f) H-TiO_{2-x} (4^{th} cycle).

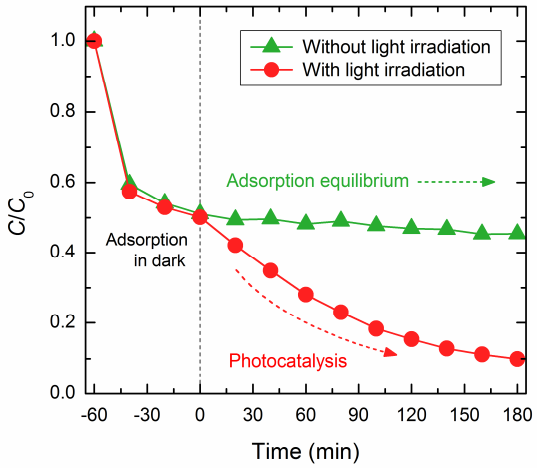

Fig. S8 MB degradation in the presence of H-TiO_{2-x} with and without visible-light irradiation.

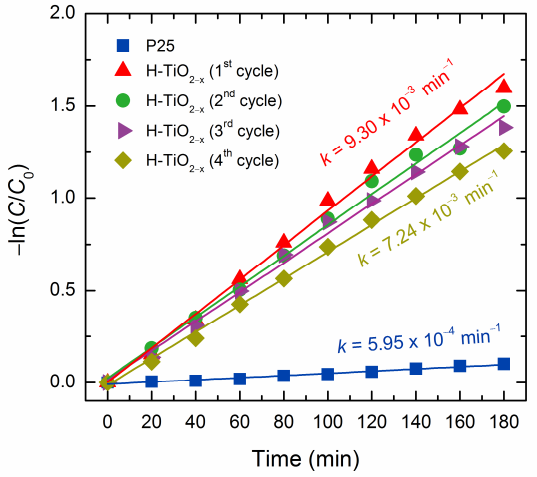

Fig. S9 Pseudo-first-order plots of $-\ln(C/C_0)$ *versus* irradiation time of the MB degradation in the presence of P25 and H-TiO_{2-x} with different cycles under visible-light irradiation. C and C_0 represent the MB concentration during the reaction time and the MB concentration after adsorption-desorption equilibrium, respectively.

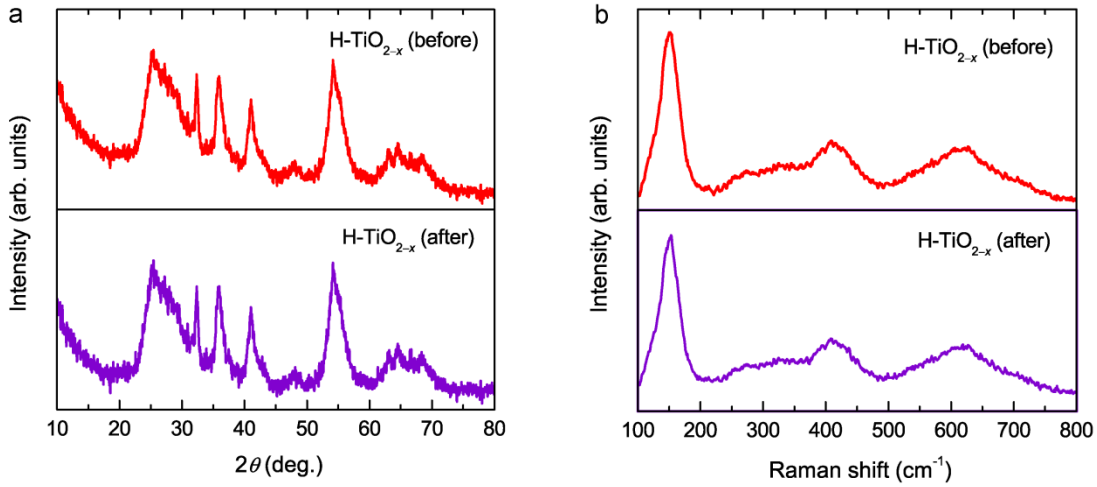

Fig. S10 (a) XRD patterns and (b) Raman spectra of H-TiO_{2-x} before and after photocatalytic test of MB degradation.

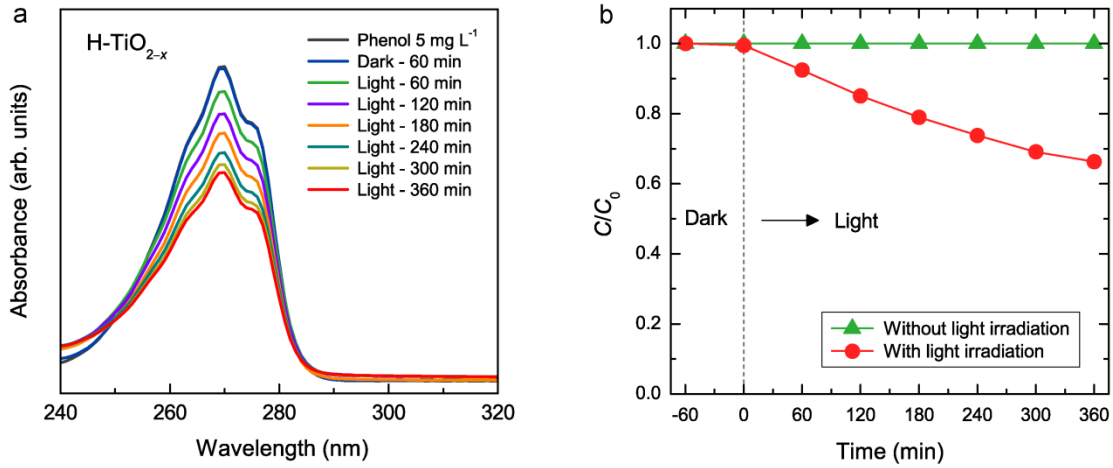

Fig. S11 (a) UV-visible absorption spectra of phenol solution in the presence of H-TiO_{2-x} at various irradiation times. (b) Phenol degradation in the presence of H-TiO_{2-x} with and without light irradiation.